Matching Reconstruction Algorithms Performance Comparison based on Compressed Sensing in GPR Imaging

Duan Rong-xing, Zhou Hui-lin and Zhu Gan-chun

School of Information Engineering, Nanchang University, Nanchang 330031, China
Zhouhuilin@ncu.edu.cn

Abstract

Compressed sensing (CS) provides a new solution for the problems of requiring large amount of measurements data and long data acquisition time in radar application, and both issues also exist in ground penetrating radar (GPR). Aiming at this problem, we adopt impulse radar with CS framework, and transform the GPR imaging into sparse constraint optimization problem performed on time-domain sub-sampling in this paper. Specifically, it focuses on the impulse GPR imaging method based on CS under double underground targets condition containing noise and abundant clutter. Furthermore, the performance of matching reconstruction algorithms under the different signal to noise ratios (SNR), measurement dimensions and sparseness values is also presented. The experimental results show that CS algorithms based on matching reconstruction can obviously reduce measurement data, improve the image quality and make a better anti-noise performance. When SNR of measurement data is 1dB, the probability of accurate imaging can still reach 95%. So we may reasonably conclude that the regularized orthogonal matching pursuit algorithm has a better performance than the other matching algorithms.

Keywords: *Compressed sensing; Ground penetrating radar imaging; Reconstruction algorithm; Matching algorithms*

1. Introduction

As a kind of effective non-destructive detection equipment, ground penetrating radar has been widely applied in various fields. Its working principle is to send high-frequency electromagnet waves to the detection zone through transmitting antenna, receive echoed signals generated in discontinuous places of underground medium via receiving antenna, and infer space distribution, structure, shape and depth information by way of signal processing [1].

In radar image, the downrange resolution depends upon $c/2B$, where c is the speed of light and B is the bandwidth of the signal, so the greater signal bandwidth, the higher downrange resolution. Besides, the crossrange resolution related to the antenna array aperture size. In order to meet increasing demands of radar image resolution, as a result, a large amount of measurements data should be sampled and long data acquisition time should be required, which have brought about huge challenge to real-time sampling system and back end processing. In recent years, a new framework, compressive sensing [2-4] (CS) has been put forward, which provides a new approach to solve large amount of data and long data acquisition time in ground-penetrating radar.

CS theory can be expressed like this: as for a sparse signal or a sparse representation in transform domain, the original signal can be recovered accurately by designing a measurement matrix meeting RIP criterion to carry out measurement with the sampling frequency far lower than that regulated by Nyquist sampling theorem and solving an optimization problem [4]. There have been several methods that apply CS for radar

imaging [5-11]. Wei has applied CS to synthetic aperture radar (SAR) imaging by a few measurements obtained high-resolution image, and analyzed the impact of the measurement matrix and noise for imaging in [5]. In [6], CS has been applied to through-wall radar imaging, and the results show that CS imaging algorithm target resolution and anti-noise performance are significantly superior to the traditional algorithm back projection (BP). In [7], Zhou has proposed a CS data acquisition and imaging method for step frequency continuous wave (SFCW) GPR, and analyzed measurement dimension and noise interference. However, it is only suitable for a single target. Although literatures [5-7] have analyzed effects of measurement matrix and noise on imaging result, they have not studied the influence of recovery algorithm on the imaging result. Besides, they have not compared the performance of recovery algorithms either. However, the recovery algorithm is the key step in CS and it will directly affect the imaging result. In [8-11], data acquisition and target reconstruction have been put forward under step frequency radar. In radar shallow detection and through-the-wall radar, pulse system radar can replace step frequency radar. Nowadays, pulse system radar has a very wide range of applications, so it has important significance to analyze the performance of CS algorithm under pulse system.

Given all that, by aiming at pulse system radar, this paper compares the imaging performance under double target conditions among orthogonal matching pursuit [12] (OMP), stagewise orthogonal matching pursuit [13] (STOMP), regularized orthogonal matching pursuit [14] (ROMP) and compressive sampling matching pursuit [15] (CoSaMP). Specifically, it focuses on the effects of sparseness, measurement dimension and noise on reconstruction algorithms under double target conditions and gives some experimental results.

2. Ground Penetrating Radar Imaging Algorithm based on CS

2.1. Simulation Scene Settings

Simulation scene settings are set as follows: the excitation signal is Ricker pulse which center frequency is $1 GHz$. the total number of time steps is $N_t = 424$. Antenna transceiver and horizontal placement, the size of simulation scenarios is $0.3m \times 0.3m$ and relative dielectric constant $\varepsilon_b = 6$, antenna placed at $y = 0$, along a line from $x = 0.05$ to $x = 0.25m$ with a step of $0.01m$. There are two point targets located at $(0.10, 0.15)$ and $(0.20, 0.15)$, which relative dielectric constant is 25 shown in Figure 1.
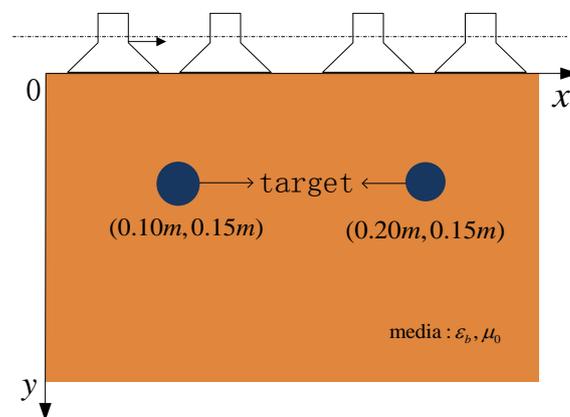

Figure 1. Simulation Scene Settings

2.2. CS Algorithms

In GPR, the target echo received by receiving antenna is the linear superposition of various target echoes and noises in the detection zone. The target echo received by antenna of group i can be defined as:

$$\mathbf{X}_i(t) = \sum_{j=0}^{M} A_j \mathbf{s}(t - \tau_j) + \mathbf{n}(t) \tag{1}$$

where i represents receiving antenna; $\mathbf{s}(t)$ means excitation signal; M indicates the target point; A_j is the amplitude of j target echo; τ_j expresses the double time delay between antenna and target and $\mathbf{n}(t)$ denotes the additive noise. Suppose that there are L groups of antennas, and then the antenna signals can be combined into a two-dimension matrix, expressed as:

$$\mathbf{B} = [\mathbf{X}_1(t)^T, \mathbf{X}_2(t)^T, \mathbf{X}_3(t)^T \ldots \mathbf{X}_L(t)^T] \tag{2}$$

In CS, the object is spare signal or signal with spare transform domain, so sparsification processing has to be carried out for signal received by the antenna. Firstly, the imaging area should be discretized and the partition grid is recorded as $\mathbf{C} = \{\pi_1, \pi_2, \pi_3 \ldots \pi_N\}$, in which N represents the number of all grid points in imaging area and two-dimensional discrete area expands into a one-dimensional by row. If the target located in π_j, then the reflection coefficient is nonzero. The sparse dictionary $\boldsymbol{\psi}$ can be expressed as:

$$[\boldsymbol{\psi}_i]_{n,j} = \frac{\mathbf{s}[t - \tau(\pi_j)]}{\left\| \mathbf{s}[t - \tau(\pi_j)] \right\|_2} \tag{3}$$

where the denominator represents the energy of the emission signal and $\tau(\pi_j)$ is the double time delay between j^{th} grid point and i^{th} group antenna. Suppose that the target appears in every grid point, and then the sparse dictionary $\boldsymbol{\psi}_i$ of the ith group antenna can be gained by Equation (3), with a size of $N_t \times N$. As for the received target echo $\mathbf{X}_i$, the sparsification processing can be carried out according to the following equation:

$$\mathbf{X}_i = \boldsymbol{\psi}_i \boldsymbol{\sigma} \tag{4}$$

where $\boldsymbol{\sigma}$ represents the reflection coefficient of the target location. In terms of the imaging result, the relative reflection coefficient $\boldsymbol{\sigma}$ of every point in the imaging area can be calculated.

In CS, instead of directly measuring signal $\mathbf{X}_i$, we measure its projection on a basis $\boldsymbol{\Phi}_i$. Measurements can be written as

$$\boldsymbol{\beta}_i = \boldsymbol{\Phi}_i \mathbf{X}_i \tag{5}$$

where $\boldsymbol{\Phi}_i$ is the measurements matrix, which size is $M \times N_t$, and $M < N_t$; M also called measurements dimension, you can find a detailed description about how to select the measurements matrix in [16]. In this paper, we use Gaussian random matrix in order to reconstruct the matrix $\boldsymbol{\sigma}$, M must satisfied the following equation [17].

$$M > K \times \log_2(N / K + 1) \tag{6}$$

Then $\boldsymbol{\sigma}$ can be achieved by solving the following convex optimization problem.

$$\boldsymbol{\sigma} = \arg\min \left\| \boldsymbol{\sigma} \right\|, \ \boldsymbol{\beta} = \boldsymbol{\Phi}\boldsymbol{\psi}\boldsymbol{\sigma} \tag{7}$$

$$\boldsymbol{\beta} = [\boldsymbol{\beta}_1{}^T, \boldsymbol{\beta}_2{}^T, \boldsymbol{\beta}_3{}^T \cdots \boldsymbol{\beta}_M{}^T]^T$$
$$\boldsymbol{\psi} = \text{diag} \ [\boldsymbol{\psi}_1, \boldsymbol{\psi}_2, \boldsymbol{\psi}_3 \cdots \boldsymbol{\psi}_M] \qquad (8)$$
$$\boldsymbol{\Phi} = [\boldsymbol{\Phi}_1{}^T, \boldsymbol{\Phi}_2{}^T, \boldsymbol{\Phi}_3{}^T \cdots \boldsymbol{\Phi}_M{}^T]$$

We select L1-magic to solve the sparse constraint optimization problem in Equation (7). Matching reconstruction algorithm based on greed mode is often used to solve Equation (5). The algorithm selects the elements that are most suitable for the measurement values from the over-complete dictionary during each time of iteration to approach the original signal via greed thought. The dictionary is updated after iteration for each time to expand the element support set till the signal can be approached via the element support set within the allowable error scope. These algorithms mainly include OMP, STOMP, ROMP and CoSaMP, and we will compare the imaging performance among these four algorithms in the following section.

3. Imaging Results and Discussions

3.1. Imaging Results

According to the simulation model parameters set in section 2.1, simulation is conducted using the numerical calculation software GprMax for electromagnetic field via FDTD. Figure 2 gives the forward modeling results.
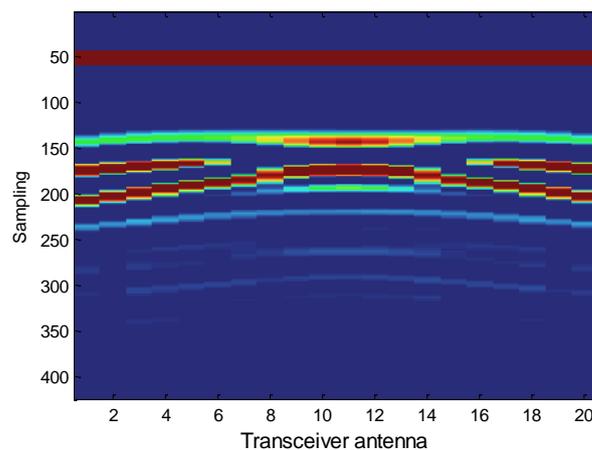

Figure 2. Impulse Radar Forward Results

The imaging area, with a size of $0.2m \times 0.3m$, is discretized and divided into 20×30 grids. Gaussian random measurement matrix is designed to carry out compression measurement for data. Sparsification is conducted for the radar forward modeling data under the complete dictionary of Equation (3). Under the noiseless conditions in which the measurement dimension $M=20$ and sparseness $K=2$, sparse dictionary, measurement matrix and measurement value are substituted into OMP, STOMP, ROMP and CoSaMP algorithms respectively. Figure 3 shows the imaging results.
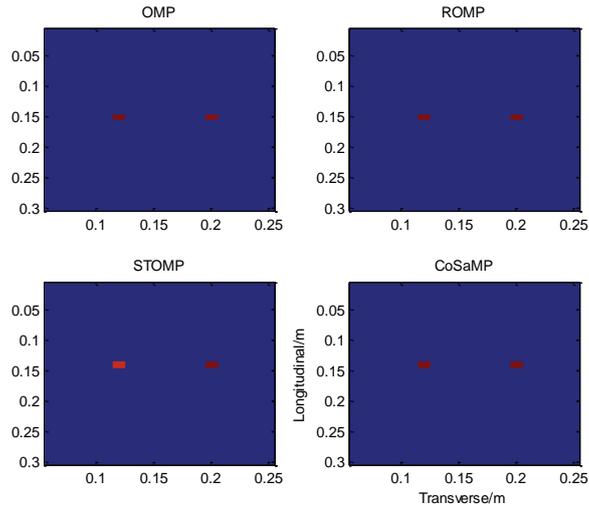
Figure 3. CS Matching Algorithms Imaging Results

CS imaging algorithm can accurately find out the target location without the redundant sidelobe jamming according to Figure 3. In the above simulations, measurement dimension, sparseness and radar data are all ideal values. In reality, we cannot predict the sparseness of the scene and optimum measurement dimension. Moreover, radar data often carry the noises. All these uncertainties will affect the imaging result. The following part will analyze how K, M and the noises have influence on the imaging result.

3.2. Effect of Sparseness

In ground penetrating radar compressed sensing imaging, iterations of the matching reconstruction algorithm are closely related to sparseness of target imaging scene, and iterations will directly affect the ultimate imaging result, so it's quite necessary to analyze the effect of sparseness on the algorithm. In the scene, two point targets are set, and the sparseness K is 2. Under the situation where the scene sparseness is unknown, if K set in the procedure is less than true K in the scene, the imaging result gained through simulation will be incomplete and not all the target locations can be found out. Figure 4 shows the imaging result of OMP algorithm (results of other algorithms are similar) when K=1. If K is greater than the true value, other redundant noises will also occur except the true target location. Figure 5 shows the imaging result of OMP algorithm when K=6.
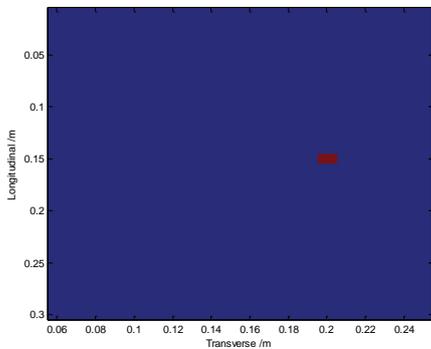

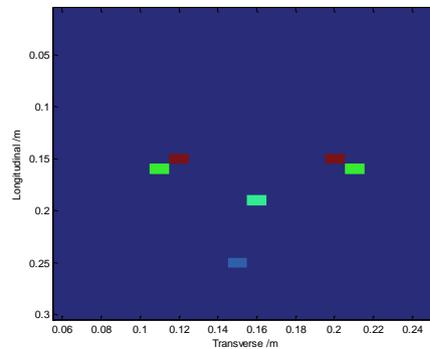**Figure 4. OMP Algorithm Imaging Results when K =1**

Figure 5. OMP Algorithm Imaging Results when K =6

According to Figure 4, when $K=1$, the imaging result only finds out one target location. When $K=6$, noises will occur around the true target location, but the true target location can still be obviously seen in the figure. Therefore, matching algorithms have a good imaging result when sparseness is unknown as long as the sparseness is greater than the true sparseness. Figure 6 presents the signal to noise ratios of the imaging results from various algorithms with the increase of K value.

As shown in Figure 6, the signal to noise ratio of the image decreases continuously with the increase of K. ROMP algorithm decreases more slowly in the signal to noise ratio compared with other algorithms, so its performance is better. Although the signal to noise ratio of the image declines, the target location can still be obviously seen according to Figure 5.
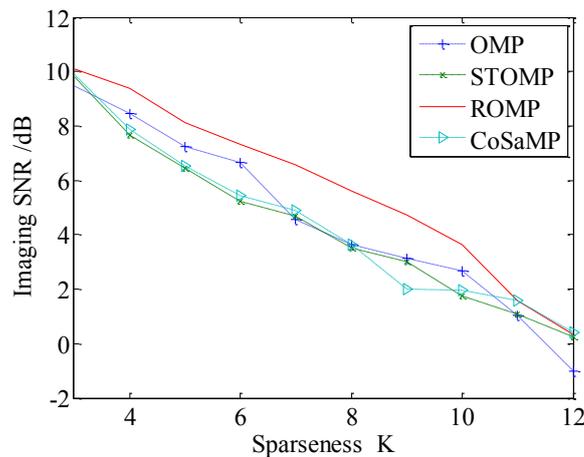

Figure 6. Effect of Sparseness

3. 3. Effect of Measurement Matrix Dimension

Gaussian random measurement matrix is adopted as the measurement matrix in this paper. According to CS theory, the measurement dimension should meet the following condition in order to accurately recover the original signal.

$$M > K \times \log_2(N / K + 1) \tag{9}$$

where K indicates the sparseness and N denotes the number of grid points in the imaging area. By substituting the simulation model parameter, we gain:

$$M > 2 \times \log_2(301) = 16.4672 \tag{10}$$

Supposing that M increases from 2 to 30, we can work out the times of the accurate imaging among the 200 simulations. The times of the accurate imaging is defined as follows. Relative dielectric constant in the imaging area is $\varepsilon_b = 6$; Ricker pulse signal, the center frequency of antenna is $1GHz$, and the formula is given according to range resolution [18]:

$$\Delta R = \frac{v}{2B} \tag{11}$$

where v indicates the propagation velocity of electromagnetic wave in the scene and B denotes the signal broadband. Substituting $\varepsilon_b = 6$ and $B = 1GHz$ in Equation (11), we can calculate $\Delta R \approx 0.03m$ by Equation (11). It is also known that the grid size of imaging scenes is $0.01m \times 0.01m$. Therefore, it can be thought as accurate imaging within one grid point extending from the true target all around. Figure 7 shows the statistics for the accurate imaging among the 200 times with the different algorithms. Figure 7 shows that when $M=17$, the probability of accurate

reconstruction reaches 95%, which meets the requirement for the measurement dimension $M > 16.4672$ in theory. According to comparison among these four algorithms, the accurate imaging probability of ROMP rises the fastest and its performance is also the best. However, with the increase of M, the computation time of CPU continues to increase. Fig. 8 shows the variation of CPU execution time with M in the 200 cycles. When $M < 20$, CPU execution time increase of various algorithms is relatively stable, but the increase is obviously accelerated after 20. This shows that the ideal value of M should be less than or equal to 20. The ideal value of M is from 17 to 20 in view of $M > 16.4672$. According to Figure 8, the CPU execution time of ROMP is lower when $M = 17\sim20$. On the basis of these factors, ROMP has better performance under different conditions of M.
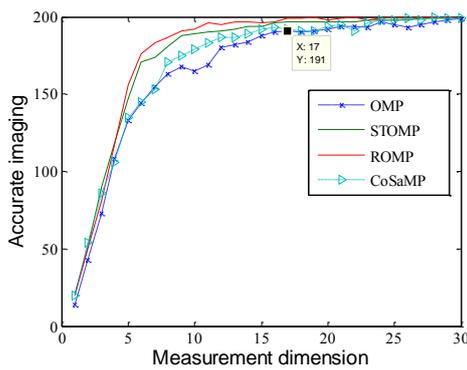

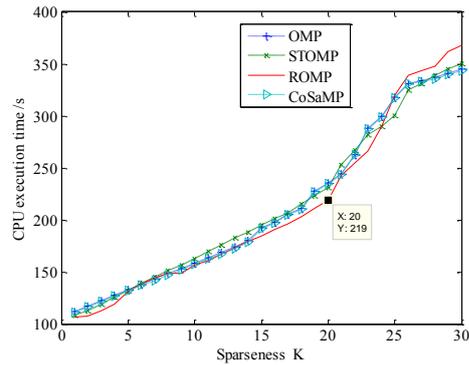**Figure 7. Effect of Measurement Matrix Dimension**

Figure 8. CPU Execution Time with the Different Sparseness

3. 4. Effect of Noises

In GPR, echo signal often carries noises, so it has important significance to analyze anti-noise performance of matching algorithms. Generally speaking, the form of echo signal in GPR can be expressed as Formula (11):

$$s_r(t) = s_d(t) + s_f(t) + s_t(t) + n(t) \tag{11}$$

where $s_d(t)$ represents the direct coupling signal among antennas; $s_f(t)$ indicates the echoed signal at stratum medium; $s_t(t)$ shows the target echo; $n(t)$ denotes the additive noise; The mathematical expression $\left| s_d(t) \right|^2 > \left| s_f(t) \right|^2 > \left| s_t(t) \right|^2$ means that the energy of the target echo is quite small when compared with $s_d(t)$ and $s_f(t)$. In the experiment, $s_d(t)$ and $s_f(t)$ are filtered out in order to better reflect the disturbance of the signal to noise ratio when the signal to noise ratio is calculated. Noises are introduced by adding small scatterers into the simulation scene. Data of the different signal to noise ratios are obtained by changing the number of scatterers and dielectric constants. The simulation has set 21 groups of the signal to noise ratio data from -10dB to 10dB. Figure 9 presents the accurate imaging statistics of various algorithms under the different signal to noise ratios.
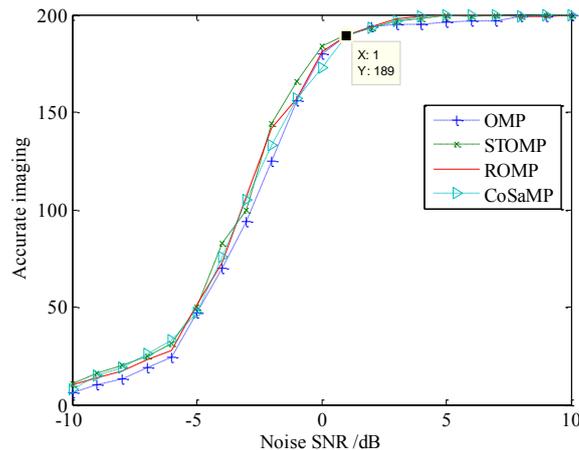
Figure 9. Effect by Noises

As shown in Figure 9, the probability of accurate imaging reaches 95% when the signal to noise ratio is 1*dB*. The simulation result shows that the matching reconstruction algorithm based on CS has quite a good anti-noise performance and it can overcome the effect of noises on the imaging result. In addition, the anti-noise performance of the four algorithms is almost the same.

4. Conclusion

This paper presents the realization process for GPR imaging algorithm based on CS and obtains the imaging results of double-target scene via OMP, ROMP, STOMP and CoSaMP reconstruction algorithms. Furthermore, the performances of various algorithms are compared under different noises environments, measurement dimensions and sparseness values. The simulation results show that CS algorithm can get a good imaging result via few measurement values, which will greatly reduce the measurement data. Moreover, the anti-noise performance of CS algorithm is also high, and when the signal to noise ratio of the measurement data is 1*dB*, the probability of accurate imaging can still reach 95%. All things considered, the regularized matching pursuit algorithm has a better overall performance compared with other matching algorithms. Its signal to noise ratio is higher during imaging under the same sparseness. In addition, the reconstruction probability is higher and CPU execution time is lower under the same measurement dimension.

Acknowledgements

References

[1]   D. J. Daniels, "Ground penetrating radar", Encyclopedia of RF and Microwave Engineering, John Wiley & Sons, Inc. Hoboken **(2005)**.
[2]   D. L. Donoho, "Compressed sensing", IEEE Transactions on Information Theory, vol. 52, no. 4, **(2006)**, pp. 1289-1306.
[3]   E. J. Candes, "Compressive sampling", Proceedings of the International Congress of Mathematicians, **(2006)**, August 22-30; Madrid, Spain, pp.1433-1452.

[4]   E. J. Candes, "The restricted isometry property and its implications for compressed sensing", Comptes Rendus Mathematique, vol. 346, no. 9, **(2008)**, pp. 589-592.

[5]   S. J. Wei, X. L. Zhang and J. Shi, "Sparse reconstruction for SAR imaging based on compressed sensing", Progress in Electromagnetics Research, vol. 109, **(2010)**, pp. 63-81.

[6]   W.-j. Zhang and M. G. Amin, "Ultrawideband impulse radar through-the-wall imaging with compressive sensing", International Journal of Antennas and Propagation, vol. 2012, **(2012)**.

[7]   L. Zhou, H.-j. Wang and Y. Su, "GPR imaging algorithm based on compressive sensing", Systems Engineering and Electronics, vol. 33, no. 9, **(2011)**, pp. 1995-2001.

[8]   A. C. Gurbuz, J. H. McClellan and W. R. Scott, "A compressive sensing data acquisition and imaging method for stepped frequency GPRs", IEEE Transactions on Signal Processing, vol. 57, no. 7, **(2009)**, pp. 2640-2650.

[9]   S. Shah, Y. Yao and A. Petropulu, "Step-frequency radar with compressive sampling (SFR-CS)", Proceedings of the IEEE International Conference on Acoustics Speech and Signal Processing, **(2010)**, 14-19 March; Dallas, USA, pp. 1686-1689.

[10] Q. Huang, L.-l. Qu, B.-h. Wu, G.-y. Fang, "UWB through-wall imaging based on compressive sensing", IEEE Transactions Geoscience and Remote Sensing, vol. 48, no. 3, **(2010)**, pp. 1408-1415.

[11] T.-d. Huang, Y.-m. Liu and H.-d. Meng, "Randomized step frequency radar with adaptive compressed sensing", Proceedings of the Radar Conference, **(2011)**, 23-27 May; Kansas, USA, pp. 411-414.

[12] T. T. Cai and L. Wang, "Orthogonal Matching Pursuit for Sparse Signal Recovery with Noise", IEEE Transactions on Information Theory, vol. 57, no. 7, **(2011)**, pp. 4680-4688.

[13] D. L. Donoho, Y. Tsaig and I. Drori, "Sparse solution of underdetermined systems of linear equations by stagewise orthogonal matching pursuit", IEEE Transactions on Information Theory, vol. 58, no. 12, **(2012)**, pp. 1094-1121.

[14] D. Needell and R. Vershynin, "Signal Recovery From Incomplete and Inaccurate Measurements Via Regularized Orthogonal Matching Pursuit", IEEE Journal of Selected Topics in Signal Processing, vol. 4, no. 2, **(2010)**, pp. 310-316.

[15] D. Needell and J. A. Tropp, "CoSaMP: Iterative signal recovery from incomplete and inaccurate samples", Applied and Computational Harmonic Analysis, vol. 26, no. 3, **(2009)**, pp. 301-321.

[16] X.-B. Li, "Research on measurement matrix based on compressed sensing", Beijing Jiaotong University, Beijing, China, **(2010)**, pp. 9-37.

[17] D. L. Donoho and Y. Tsaig, "Extensions of compressed sensing", Signal Processing, vol. 86, no. 3, **(2006)**, pp. 533-548.

[18] G.-l. Cui, "Ultra-wideband wall radar synthetic aperture imaging algorithm research and implementation", University of electronic science and technology of China, Chengdu, China**, (2008),** pp. 6-9.